Optics Letters

Switchable Pancharatnam–Berry microlens array with nano-imprinted liquid crystal alignment

Ziqian He,[1] Yun-Han Lee,[1] Ran Chen,[1] Debashis Chanda,[1,2,3,4] and Shin-Tson Wu[1,*]

[1]College of Optics and Photonics, University of Central Florida, Orlando, Florida 32816, USA
[2]Department of Physics, University of Central Florida, Orlando, Florida 32816, USA
[3]NanoScience Technology Center, University of Central Florida, Orlando, Florida 32826, USA
[4]e-mail: Debashis.Chanda@creol.ucf.edu
*Corresponding author: swu@creol.ucf.edu

Received 30 July 2018; revised 11 September 2018; accepted 14 September 2018; posted 17 September 2018 (Doc. ID 340679); published 10 October 2018

We report a rapid nano-imprinting technique to pattern the liquid crystal alignment of a Pancharatnam–Berry phase microlens array. Through implementing a single-side aligned cell, we demonstrate a switchable microlens array with fast response time and low operation voltage. Further investigation of focusing property as well as imaging capability ensure the good quality of the microlens array. Besides planar structures, this method is also promising for patterning liquid crystal alignment on curvilinear surfaces.

OCIS codes: (220.1140) Alignment; (230.3720) Liquid-crystal devices; (050.1965) Diffractive lenses; (220.4241) Nanostructure fabrication.

https://doi.org/10.1364/OL.43.005062

An active liquid crystal (LC) microlens array is an essential electro-optical device for many applications, including image processing [1–5], beam steering [6,7], wavefront correction [8], and switchable 2D/3D displays [9–11]. Compared to the refraction-type active LC microlens arrays, the diffractive ones are more compact, and the response time is usually faster due to the thinner cell gap. Therefore, for applications which require only on/off switches, the diffractive-type microlens array has its merits.

Recent advances in the development of Pancharatnam–Berry (PB) phase optical elements draw great attention to creating new diffractive optical components [12,13]. Unlike the traditional dynamic phase produced via optical path difference, PB phase corresponds to the phase shift introduced by the changes in other light wave parameters [14,15]. A well-known method for creating PB phase is by patterning half-wave plates in a space-variant manner. If the optical axis is denoted as $\varphi(x, y)$ and the common phase term is ignored, with a circularly polarized input light, the output light can be calculated by the Jones matrix as [16]

$$J_{\pm} = \frac{1}{\sqrt{2}} \begin{bmatrix} \cos 2\varphi & \sin 2\varphi \\ \sin 2\varphi & -\cos 2\varphi \end{bmatrix} \begin{bmatrix} 1 \\ \pm i \end{bmatrix} = \frac{1}{\sqrt{2}} \begin{bmatrix} 1 \\ \mp i \end{bmatrix} e^{\pm 2i\varphi}. \quad (1)$$

Equation (1) indicates that the angle of the local optical axis $\varphi(x, y)$ will impart a $2\varphi(x, y)$ phase delay to the input light. This unique property of PB phase is useful for generating arbitrary wavefronts, such as PB lenses. Typically, to fabricate a LC PB lens, several approaches can be applied to introduce the desired alignment with photoalignment materials, such as interference exposure [17,18], direct scanning [19], and projection lithography [20]. But for a microlens array with a relatively short focal distance, few studies have been reported. The interference exposure method is limited by the bulkiness of the beamsplitter and the exposure accuracy. The direct scanning method is mainly restricted by the laser beam size and the total patterning size, while the projection lithography approach is the most promising method, which is mostly subjected to the pixel size of the spatial light modulators. Another interesting phenomenon is that the LC alignment of a PB lens can be recorded through another PB lens with linearly polarized input light. A noteworthy property of this technique is the doubled spatial frequency of the recorded alignment compared to the applied template [21]. Assisted with a 2D mechanical stage, a lens array can be achieved [22]. The major shortcomings of this method include the slow processing speed due to the series of exposure, a high precision mechanical stage needed especially for small-size lens arrays, and multiple reflections in the substrate and between different substrates which distort the recorded alignment. Therefore, a new fabrication technique is needed for achieving switchable PB microlens arrays.

In this Letter, we propose a rapid method to pattern LC alignment of a PB microlens array by nanoimprint lithography (NIL) [23]. Previously, NIL has been used to fabricate uniform homogeneous, homeotropic, and degenerate LC alignments [24,25]. Here instead, NIL is applied to pattern space-variant homogeneous LC alignment. The alignment pattern contains a group of submicrometer period gratings whose orientation rotates in-plane, according to the design requirement. By implementing a single-side aligned LC cell, we demonstrate a fast-switching PB microlens array. The focusing property and the imaging capability are investigated. This new technique is promising for a rapid replication of arbitrary planar alignment.

Figure 1 illustrates the schematic of our device design. From Fig. 1(a), the LC cell only has single-side alignment on the bottom substrate. The periodicity of alignment, P, is 148 μm, and the fill fraction is approximately 100%. The ideal pattern of the LC directors for a single microlens is depicted in Fig. 1(b), which can be described as

$$\varphi(x,y) = -\frac{\pi}{\lambda}\left(\sqrt{x^2+y^2+f^2}-f\right), \quad (2)$$

where λ and f are the designed wavelength and focal length, respectively. Translating the LC director distribution to grating alignment is simple, because the grating offers homogeneous alignment along the grooves [26–28]. Therefore, the direction of grooves is essentially the same as the LC director distribution. In our case, NIL is utilized to generate the 2D planar alignment pattern. But in general, this method can be applied to create alignment on other curvilinear surfaces [29] by casting stamps accordingly.

To generate the LC molecular alignment pattern, a polymer dimethylsiloxane (PDMS; Dow Corning Sylgard) stamp was first cast from a master which was made by two-photon polymerization based direct-laser writing (NanoScribe GmbH). To fulfil NIL, a thin film of SU-8 2000.5 (MicroChem) was spun upon an ITO-coated glass substrate at 500 rpm for 5 s followed by 3000 rpm for 30 s, and then prebaked at 95°C for 1 min. This film was then imprinted with the polymer stamp on a hotplate at 95°C for 20 s. After removing the substrate with the stamp from the hotplate and letting it cool down for 30 s, the stamp was gently delaminated from the substrate. Last, the substrate was UV cured for 5 min and postexposure baked at 95°C for 5 min. To finish the cell, a single-side ITO-coated glass superstrate without alignment was adhered to the bottom substrate using NOA 81, with sparsely distributed silica spacers to control the cell gap (1.6 μm). Once UV cured, the cell was then filled with a LC mixture MLC-14200 (Merck), which has $\Delta n = 0.17$ at $\lambda = 633$ nm, $\Delta\epsilon = 30.4$ at 1 kHz driving frequency, $\gamma_1/K_{11} = 27.77$ ms/μm^2 at room temperature (γ_1 is the rotational viscosity and K_{11} is the splay elastic constant). It is worth mentioning that the single-side alignment works when the anchoring force is strong and the cell gap is thin.

Figure 2(a) shows the designed phase profile for a circularly polarized light along the a axis as Fig. 1(b) depicts. The alignment pattern was designed in a discrete sense that there are at least five zones within 180° rotation of the alignment direction. For each zone, the LC alignment is uniformly oriented at a direction, determined by the ideal phase profile at that zone center. The corners of the microlens array are also utilized, resulting in a nearly 100% fill factor. The intensity profile of the focal point by this digitization is calculated as Fig. 2(b) shows, where it is plotted along the x axis in the focal plane. To clarify, the calculation is based on a single microlens with Fresnel and thin-lens approximations, and the target wavelength is 532 nm. By this digitization, the peak intensity dropped by 10.4%, as compared to the continuous case.

Figures 3(a)–3(c) show the morphology of the imprinted alignment pattern, which was observed under scanning electron microscopy (SEM) (Zeiss ULTRA-55 FEG SEM). As noted in Fig. 3(b), unlike a perfect digitization, some empty spaces between different zones were also designed to let LC molecules freely rotate in between. The detail of the grooves is demonstrated in Fig. 3(c). The groove alignment has 600-nm period and around 100-nm groove depth, which can provide anchoring energy at the level of several μJ/m^2. After the finish of the cell, we used polarized optical microscopy (POM) with a 546-nm interference color filter to evaluate the molecular alignment quality. As noted in Fig. 3(d), it turns out that the single-side

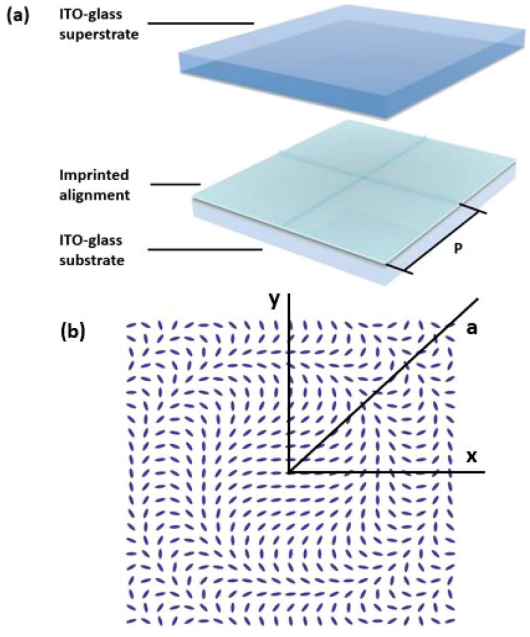

Fig. 1. (a) Schematic of the single-side aligned PB microlens array where P denotes the periodicity of the microlens array. (b) Ideal distribution of the LC directors for a single microlens.

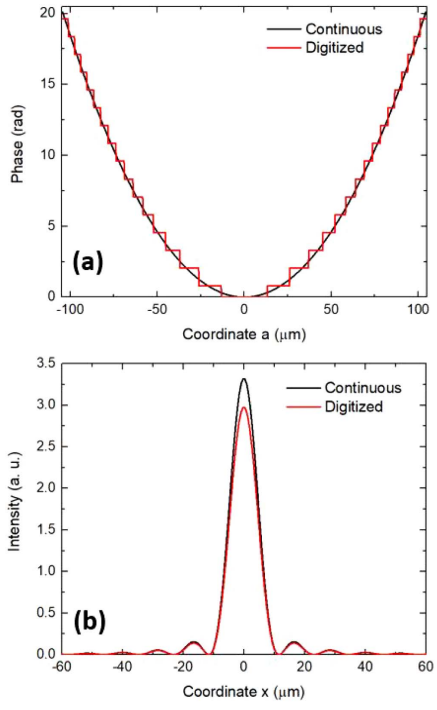

Fig. 2. (a) Phase profile along a axis for both the continuous case and the digitized case. (b) Calculated intensity profile along x axis in the focal plane for both cases.

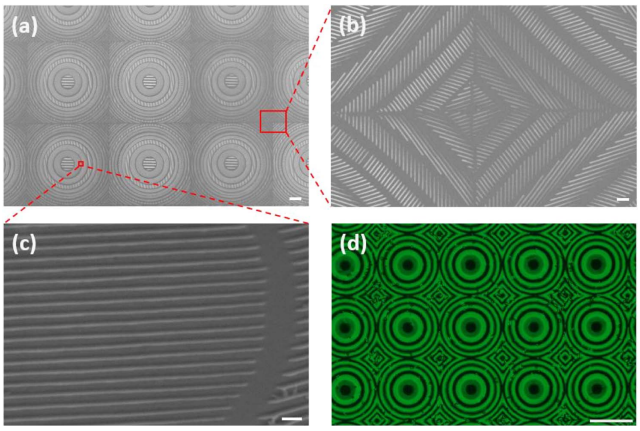

Fig. 3. (a) SEM image of the imprinted alignment of a 20 × 20 microlens array where each microlens is 148 μm × 148 μm. (b) Details at the boundary between microlenses. (c) Details of the grooves where the line period is 600 nm, and the depth of the grooves is around 100 nm. (d) POM image of the 20 × 20 microlens array cell. Scale bar: 20 μm (a), 2 μm (b), 1 μm (c), and 100 μm (d).

alignment cell is capable of aligning LC molecules while some defects still exist. The defects arise from several factors, including the misalignment caused by using only single-side alignment, some defects of the imprinted alignment pattern itself during the transfer, and the formation of some random LC domains.

We further extracted the phase profile of a single microlens for one circular polarization, as plotted in Fig. 4, where $\lambda = 546$ nm. As Fig. 4(b) indicates, our fabricated microlens shows a discrete profile and the phase at corners deviates severely from the ideal phase profile, which means the anchoring energy at the corners is not strong enough.

Next, we used an optical microscope (OLYMPUS BX51) to measure the focal length of the PB microlens array. Through the stage height adjustment from the substrate to the clear focal points, the focal length can be directly read out from the scale of the microscope. In experiment, we utilized three different interference color filters ($R = 633$ nm, $G = 546$ nm, and $B = 450$ nm) to measure the dispersion of the focal length. The measured focal length is around ±2.49 mm for B, ±2.84 mm for G, and ±3.40 mm for R, respectively, where the error of measurement is ±0.15 mm due to the finite depth of focus. The two focal points on different sides of the cell correspond to two orthogonal circular polarizations of light. The focus of the PB microlens array disappears totally when the applied voltage reaches 8 V_{rms}.

One merit of the PB microlens array, in comparison with traditional refractive LC microlens array, is its relatively fast response time due to the thinner cell gap. When releasing the applied voltage at 8 V_{rms}, the decay time (100% to 10% transmittance change) is measured as 3.57 ms.

The focusing property of the PB microlens array at three specified wavelengths is illustrated in Fig. 5. For all three wavelengths, the designed PB microlens array can generate well-defined focal points. Without the circular polarizer, the image consists of converged focal points and diverged background signals, corresponding to the different behaviors of the two orthogonal circular polarizations. In the presence of a circular polarizer, the contrast is readily improved. The optical efficiency, defined as the ratio of the optical power of the focused beam to that of the circularly polarized incident beam, at voltage-off stage is 47.2% for 633 nm, 57.6% for 546 nm, and 52.2% for 450 nm. As can be seen, the background signal still exists even with a circular polarizer, due to multiple factors, such as digitized phase profile, diffraction introduced by the array, and random line defects of LC molecules.

Another important aspect of microlenses is the imaging capability. Figure 6 summarizes the white-light (yellowish halogen light source) imaging quality and the switching ability of the PB microlens array without the circular polarizer. The targets were 5.5 mm away from the substrate of the cell, and the images were collected using the abovementioned optical microscope with a 5× objective and an Infinity 2-2 camera. As mentioned, the PB microlens has two focal points, corresponding to two circular polarizations. Here we only characterized the imaging capability of the concave microlens, which corresponds to the one with negative focal length. In experiment, three imaging targets, including "UCF" letters [Fig. 6(a)], the four-dot target [Fig. 6(b)], and the three-bar target [Fig. 6(c)], were used. At voltage-off state, the three-bar target with 40.3 lp/mm resolution can be clearly resolved. The four-dot target can also be separated well, and the shape of the dots remained. To clarify, the inset red dashed rectangle in Fig. 6(b) denotes one image of the four-dot target. "UCF" letters were applied to demonstrate the imaging of a noncentrosymmetric pattern, and the letters can be recognized well. As noticed, there are

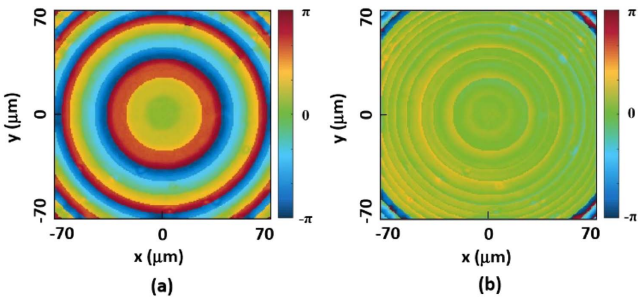

Fig. 4. (a) Extracted phase profile of the fabricated single microlens, where $\lambda = 546$ nm. (b) Difference between the ideal phase profile and the extracted phase profile.

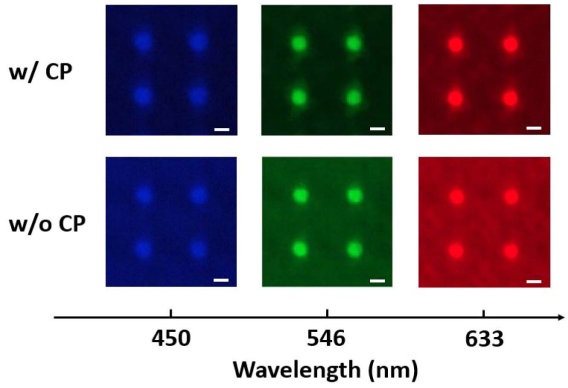

Fig. 5. Focusing property of the fabricated PB microlens array at three specified wavelengths. From top to bottom: with a circular polarizer and without the circular polarizer. Scale bar: 20 μm for all.

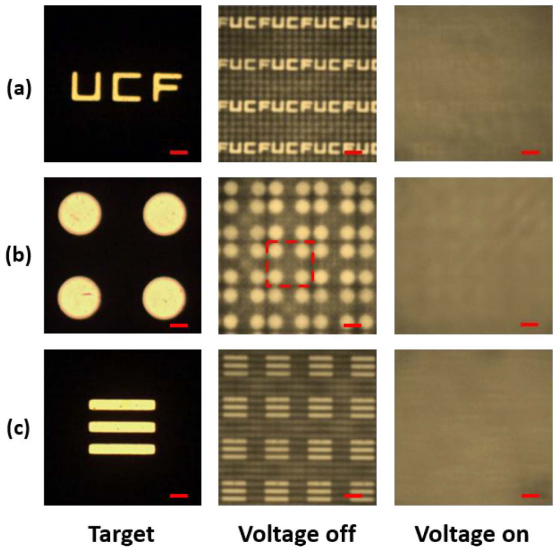

Fig. 6. White-light imaging capability of the PB microlens array for different targets. From top to bottom: (a) "UCF" letters, (b) the four-dot target, and (c) the three-bar target. The inset red dashed rectangle in (b) denotes a single four-dot image formed by the PB microlens array. The applied voltage at voltage-on state is 8 V_{rms}. Scale bar: 20 μm for all.

some background noises on the image plane. This is due to the disturbance of the other circularly polarized light as well as the reasons discussed above in Fig. 5. To illustrate the switching ability, we applied 8 V_{rms} to the cell. As shown in Fig. 6, all the images at voltage-on state were almost indiscernible.

In conclusion, we demonstrate a rapid method to pattern the LC alignment for a PB microlens array. This NIL based grating alignment can provide anchoring force to LC molecules, validated through SEM and POM characterization. By implementing a single-side aligned cell, we demonstrate that the switching time is 3.57 ms and the working voltage is 8 V_{rms}. Further investigations of the focusing property and the imaging capability ensure good quality of the PB microlens array. The NIL-based method is not only suitable for 2D planar alignment patterning but also promising for patterning LC alignment on other curvilinear surfaces.

Funding. Air Force Office of Scientific Research (AFOSR) (FA9550-14-1-0279); National Science Foundation (NSF) (ECCS-1509729).

Acknowledgment. We thank Sushrut Modak and Dr. Daniel Franklin for the help with NIL and Tao Zhan for helpful discussions.

REFERENCES

1. T. Nose, S. Masuda, S. Sato, J. Li, L.-C. Chien, and P. J. Bos, Opt. Lett. **22**, 351 (1997).
2. H. Ren and S.-T. Wu, Appl. Phys. Lett. **82**, 22 (2003).
3. Y. H. Lin, Y. J. Wang, and V. Reshetnyak, Liq. Cryst. Rev. **5**, 111 (2017).
4. A. Orth and K. Crozier, Opt. Express **20**, 13522 (2012).
5. P.-Y. Hsieh, P.-Y. Chou, H.-A. Lin, C.-Y. Chu, C.-T. Huang, C.-H. Chen, Z. Qin, M. M. Corral, B. Javidi, and Y.-P. Huang, Opt. Express **26**, 10981 (2018).
6. S. Masuda, S. Takahashi, T. Nose, S. Sato, and H. Ito, Appl. Opt. **36**, 4772 (1997).
7. A. Akatay, C. Ataman, and H. Urey, Opt. Lett. **31**, 2861 (2006).
8. L. Hu, L. Xuan, D. Li, Z. Cao, Q. Mu, Y. Liu, Z. Peng, and X. Lu, J. Opt. A **11**, 015511 (2009).
9. J.-H. Na, S. C. Park, S.-U. Kim, Y. Choi, and S.-D. Lee, Opt. Express **20**, 864 (2012).
10. J. F. Algorri, V. Urruchi, J. M. Sánchez-Pena, and J. M. Otón, J. Disp. Technol. **10**, 713 (2014).
11. J. F. Algorri, V. Urruchi, B. García-Cámara, and J. M. Sánchez-Pena, Materials **9**, 36 (2016).
12. E. Hasman, V. Kleiner, G. Biener, and A. Niv, Appl. Phys. Lett. **82**, 328 (2003).
13. S. R. Nersisyan, N. V. Tabiryan, D. M. Steeves, and B. R. Kimball, Opt. Photon. News **21**(3), 40 (2010).
14. S. Pancharatnam, Proc. Indian Acad. Sci. A **44**, 247 (1956).
15. M. V. Berry, Proc. R. Soc. London A **392**, 45 (1984).
16. Y. H. Lee, G. Tan, T. Zhan, Y. Weng, G. Liu, F. Gou, F. Peng, N. V. Tabiryan, S. Gauza, and S. T. Wu, Opt. Data Process. Storage **3**, 79 (2017).
17. J. Kim, Y. Li, M. N. Miskiewicz, C. Oh, M. W. Kudenov, and M. J. Escuti, Optica **2**, 958 (2015).
18. C. Yousefzadeh, A. Jamali, C. McGinty, and P. J. Bos, Appl. Opt. **57**, 1151 (2018).
19. M. N. Miskiewicz and M. J. Escuti, Opt. Express **22**, 12691 (2014).
20. L. De Sio, D. E. Roberts, Z. Liao, S. Nersisyan, O. Uskova, L. Wickboldt, N. Tabiryan, D. M. Steeves, and B. R. Kimball, Opt. Express **24**, 18297 (2016).
21. S. R. Nersisyan, N. V. Tabiryan, D. M. Steeves, and B. R. Kimball, Appl. Opt. **48**, 4062 (2009).
22. S. V. Serak, D. E. Roberts, J.-Y. Hwang, S. R. Nersisyan, N. V. Tabiryan, T. J. Bunning, D. M. Steeves, and B. R. Kimball, J. Opt. Soc. Am. B **34**, B56 (2017).
23. S. Y. Chou, P. R. Krauss, and P. J. Renstrom, Science **272**, 85 (1996).
24. Y. Yi, M. Nakata, A. R. Martin, and N. A. Clark, Appl. Phys. Lett. **90**, 163510 (2007).
25. H. G. Park, J. J. Lee, K. Y. Dong, B. Y. Oh, Y. H. Kim, H. Y. Jeong, B. K. Ju, and D. S. Seo, Soft Matter **7**, 5610 (2011).
26. C.-H. Lee, H. Yoshida, Y. Miura, A. Fujii, and M. Ozaki, Appl. Phys. Lett. **93**, 173509 (2008).
27. Y.-H. Lee, D. Franklin, D. Chanda, F. Gou, F. Peng, G. Liu, and S.-T. Wu, Sci. Rep. **7**, 16260 (2017).
28. Z. He, Y.-H. Lee, F. Gou, D. Franklin, D. Chanda, and S.-T. Wu, Opt. Express **25**, 33688 (2017).
29. Z. He, Y.-H. Lee, D. Chanda, and S.-T. Wu, Opt. Express **26**, 21184 (2018).